4. Mayberry JC, Ham LB, Schipper PH, Ellis TJ, Mullins RJ. Surveyed opinion of American trauma, orthopedic, and thoracic surgeons on rib and sternal fracture repair. J Trauma 2009;66:875–9.
5. Metzelder ML, Kuebler JF, Leonhardt J, Ure BM, Petersen C. Self and parental assessment after minimally invasive repair of pectus excavatum: lasting satisfaction after bar removal. Ann Thorac Surg 2007;83:1844–9.

High-Speed 3-Dimensional Imaging in Robot-Assisted Thoracic Surgical Procedures

Naohiro Kajiwara, MD, Soichi Akata, MD, Masaru Hagiwara, MD, Koichi Yoshida, MD, Yasufumi Kato, MD, Masatoshi Kakihana, MD, Tatsuo Ohira, MD, Norihiko Kawate, MD, and Norihiko Ikeda, MD

Departments of Surgery and Radiology, Tokyo Medical University, Tokyo, and Department of Health Science and Social Welfare, Waseda University School of Human Sciences, Saitama, Japan

We used a high-speed 3-dimensional (3D) image analysis system (SYNAPSE VINCENT, Fujifilm Corp, Tokyo, Japan) to determine the best positioning of robotic arms and instruments preoperatively. The da Vinci S (Intuitive Surgical Inc, Sunnyvale, CA) was easily set up accurately and rapidly for this operation. Preoperative simulation and intraoperative navigation using the SYNAPSE VINCENT for robot-assisted thoracic operations enabled efficient planning of the operation settings. The SYNAPSE VINCENT can detect the tumor location and depict surrounding tissues quickly, accurately, and safely. This system is also excellent for navigational and educational use.

(Ann Thorac Surg 2014;97:2182–4)

FEATURE ARTICLES

We previously reported on the importance of appropriate settings in robot-assisted thoracic surgical procedures, because no target is located in the same location within the thoracic cavity [1, 2]. Moreover, once all the da Vinci S (Intuitive Surgical, Inc, Sunnyvale, CA) devices and equipment are positioned, it is difficult to reset the da Vinci S after the operator starts manipulation through the operator console. In this case, a high-speed 3-dimensional (3D) image analysis system, the SYNAPSE VINCENT (Fujifilm Corp, Tokyo, Japan), was used to determine the best positioning of robot arms and instruments preoperatively based on experience with more than 100 video-assisted thoracic operations. Moreover, this system can detect the tumor location and depict surrounding tissues—even 1-mm vessels—quickly, accurately, and safely. An incision for the 3D camera and 2 other incisions are made at the appropriate points according to the SYNAPSE VINCENT analysis. The best angulation of the instrument arms of the da Vinci S are also determined by the same analysis. All computed tomography (CT) must satisfy several conditions necessary to analyze images by the SYNAPSE VINCENT. First, all images are to be taken by multislice CT at more than 64 lines; second, all images are taken at a slice interval thickness of 1.25 mm; third, all image data are saved as digital imaging and communication in medicine (DICOM) image files; and fourth, all images are to be taken using contrast media. The SYNAPSE VINCENT also provides more information concerning tumor size and shape and also whether the tumor invades surrounding tissue and the extent of airway and vessel involvement.

A 38-year-old woman had a posterior mediastinal tumor that appeared spindle-shaped at the upper level of the first to third thoracic vertebrae. The SYNAPSE VINCENT was used to define the tumor together with the surrounding anatomic information and determine the appropriate setting of the da Vinci S and the best positioning of the instrument ports. For the computed tomographic scan, the patient was placed in the same position as projected for the operation. The SYNAPSE VINCENT depicts the tumor and all other anatomic information quickly. Details of thorax, ribs, and virtual imaging of the robot arm directions and placement of the surgical ports are shown in Fig 1. Details of the tumor and surrounding vessels after removal of the image of the rib cage are shown in Fig 2. The direction of the da Vinci S, 3D camera setting, and positioning of arms No. 1 and No. 2 for the clinical operation were determined by

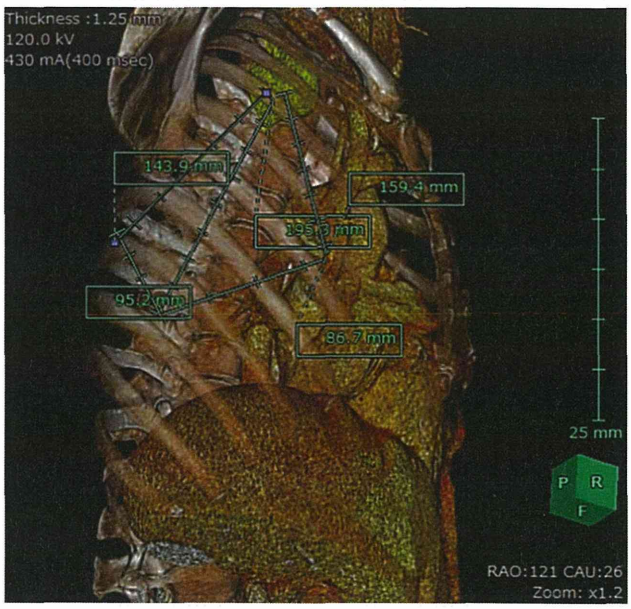

Fig 1. The figures were depicted by the SYNAPSE VINCENT, which showed the tumor (yellow) located in the upper area in the right side of the thorax. Green points on the surface of the patient and lines show the appropriate approaches for the instrument ports and angles of the arms of the da Vinci S and distance of each interval.

Accepted for publication Aug 8, 2013.

Address correspondence to Dr Kajiwara, Department of Surgery, Tokyo Medical University, 6-7-1 Nishishinjuku, Shinjuku-ku, Tokyo 160-0023, Japan; e-mail: naokjw@topaz.ocn.ne.jp.

0003-4975/$36.00
http://dx.doi.org/10.1016/j.athoracsur.2013.08.026

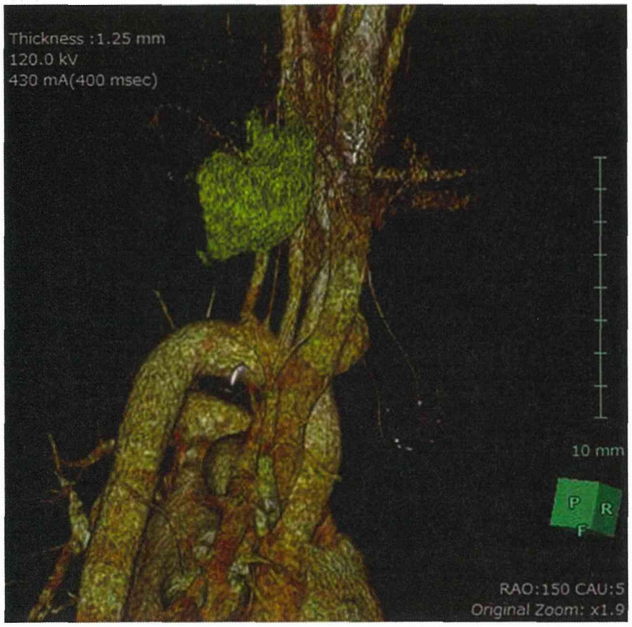

Fig 2. Details of the tumor and surrounding vessels after removal of the image of the rib cage.

preoperative simulation using the SYNAPSE VINCENT (Fig 3). The da Vinci S was rolled in from the 1 o'clock direction, as shown in Fig 3. The patient was placed in a semisupine position. The 3D camera port was placed in the area of the sixth intercostal space at the anterior axillary line. Arms No. 1 and No. 2 and the accessory port were placed in the area of the fifth intercostal space at the anterior axillary line, the sixth intercostal space at the posterior axillary line, and the seventh intercostal space at the anterior axillary line, respectively. Fig 1 shows the 3D anatomic structure of the patient, the suitable points for each instrument port, and the intervals between each point. The distances from the tumor to the point of the instrument port of arms No. 1 and No. 2 and the 3D camera were 143.9 mm, 159.4 mm, and 195.3 mm, respectively. The distances from the 3D camera to the points of the instrument port of arms No. 1 and No. 2 were 95.2 mm and 86.7 mm, respectively.

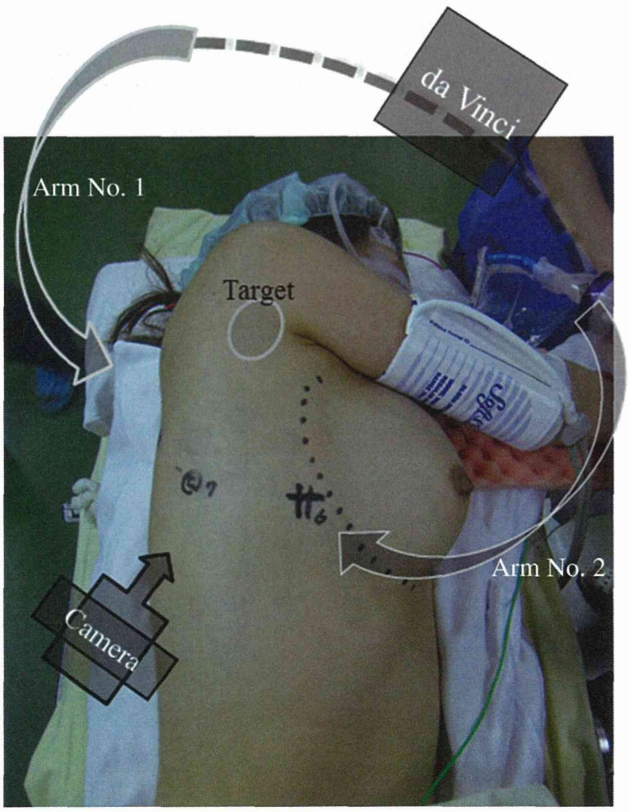

Fig 3. The da Vinci S was rolled in from the 1 o'clock direction, with the patient located between arms No. 1 and No. 2.

The da Vinci S was set up accurately and rapidly for this operation (about 10 minutes until the robot roll-in). The total operation time was 270 minutes, the robot set-up time was 21 minutes, and the console time (the robot working time) was 132 minutes. The amount of bleeding was 167 mL, and the drainage time was 2 days after the operation. The patient had no complications, and slight pain on the visual analogue scale (range 0–10) was a maximum of 1 at the time of discharge from the hospital. The pathologic report revealed a schwannoma (85 × 42 × 20 mm) with no malignancy.

Comment

Robotic operations using the da Vinci S has been approved in various specialties. However, thoracic tumors can be located at various sites in individual cases. In particular, the crucial factors for successful procedures in robot-assisted thoracic operations are the selection of the appropriate placement and the angle of instrument ports selected individually in relation to the target and patient position, which varies according to the tumor location [1, 2]. The distance separating each instrument port is at least 8 cm to prevent interference from other arms. Furthermore, the distance separating each instrument port from the target is at least 10 to 20 cm to secure a sufficient working space within the thoracic cavity.

The recent development of the SYNAPSE VINCENT raises the issue of whether it can yield comparable results in speed and precision. Mochizuki and colleagues [3] and Ikeda and associates [4] reported the feasibility and safety of the SYNAPSE VINCENT in performing useful preoperative simulation and navigation of surgical procedures [5]. It is safer, more precise, and less invasive for the patient, and it is easy to construct an image, depending on the purpose, in 5 to 10 minutes using the SYNAPSE VINCENT. Moreover, if the lesion is in the parenchyma, it helps to perform simulation with virtual skeletal subtraction to estimate potential lesion movement. It also helps to remember that even in such cases, most vascular structures will not move significantly. Because the angle of the 3D image made by the SYNAPSE VINCENT can be changed freely on a personal computer, an angle image similar to the

operation field in the surgical procedure could easily be obtained as a simulation image. Constructed images are displayed in the operating room on a monitor, which can be used for deciding surgical strategy and for navigation during intraoperative surgical manipulation.

Preoperative simulation using the SYNAPSE VINCENT also reduces the surgeon's stress levels, particularly when highly skilled techniques are needed to operate on lesions in difficult to reach and widely spaced areas of the thoracic cavity. This task, including both preoperative simulation and intraoperative navigation, could lead to greater safety and precision in operative settings and manipulation by creating the appropriate port positioning and direction of the instrument arms. These technologic instruments should be helpful for robot-assisted thoracic operations by thoracic surgeons and are also excellent devices for educational training.

The authors are grateful to Associate Professor Edward Barroga and Professor Emeritus J. Patrick Barron, of the Department of International Medical Communications of Tokyo Medical University, for their editorial review of the English manuscript.

References

1. Kajiwara N, Kakihana M, Kawate N, Ikeda N. Appropriate set-up of the da Vinci Surgical System in relation to the location of anterior and middle mediastinal tumors. Interact Cardiovasc Thorac Surg 2011;12:112–6.
2. Kajiwara N, Kakihana M, Usuda J, Ohira T, Kawate N, Ikeda N. Extended indications for robotic surgery for posterior mediastinal tumors. Asian Cardiovasc Thorac Ann 2012;20:308–13.
3. Mochizuki K, Takatsuki M, Soyama A, Hidaka M, Obatake M, Eguchi S. The usefulness of a high-speed 3D-image analysis system in pediatric living donor liver transplantation. Ann Transplant 2012;17:31–4.
4. Ikeda N, Yoshimura A, Hagiwara M, Akata S, Saji H. Three dimensional computed tomography lung modeling is useful in simulation and navigation of lung cancer surgery. Ann Thorac Cardiovasc Surg 2013;19:1–5.
5. Inoue T, Kitamura Y, Li Y, Ito Y. Robust airway extraction based on machine learning and minimum spanning tree. Proceedings of the Society for Optics and Photonics (SPIE) 2013;8670:6700L.

FEATURE ARTICLES

Treatment of Giant Pharyngoesophageal Diverticulum by Video-Assisted Thoracoscopy

Xun Zhang, MD, Shizhao Cheng, MD, Yijun Xu, MD, and Shunhua Wang, MD

Department of Thoracic Surgery, Tianjin Chest Hospital, Tianjin, China

A 67-year-old woman presented with a giant pharyngoesophageal diverticulum (Zenker's diverticulum) that extended deep into the chest. Surgery, using either an open or endoscopic approach, was difficult. We stapled the common wall between the diverticulum and the esophagus using video-assisted thoracoscopic surgery. The patient exhibited good anatomic and functional results at 6 months' follow-up.

(Ann Thorac Surg 2014;97:2184–6)

Pharyngoesophageal diverticulum (Zenker's diverticulum) is a protrusion of pharyngeal mucosa between fibers of the lower pharyngeal constrictor and cricopharyngeal muscles. Treatment of massive Zenker's diverticulum is a challenge. Open surgical approaches require extensive dissection of the diverticulum, which greatly increases the morbidity and mortality rate. Endoscopic surgery, however, can leave an incomplete common wall transection, leading to persistent dysphagia and vomiting. We report a case of an elderly patient with a giant Zenker's diverticulum successfully treated with video-assisted thoracoscopic surgery.

A 67-year-old woman presented with a sore throat and vomiting for the previous 6 months. She also had progressive dysphagia (for both solid and liquid foods) with weight loss for the previous 6 years. The results of a routine physical examination were unremarkable. A barium swallow test showed significant retention of barium in a massive Zenker's diverticulum reaching the carina (10.0 × 6.0 cm), with minimal conduction of barium into the distal esophageal lumen (Fig 1A). A computed tomographic scan revealed a right-sided large pouch with an air-fluid level. The trachea was deviated anteriorly. Profound stenosis of the esophagus was also noted. An upper gastrointestinal endoscopy revealed a pharyngeal

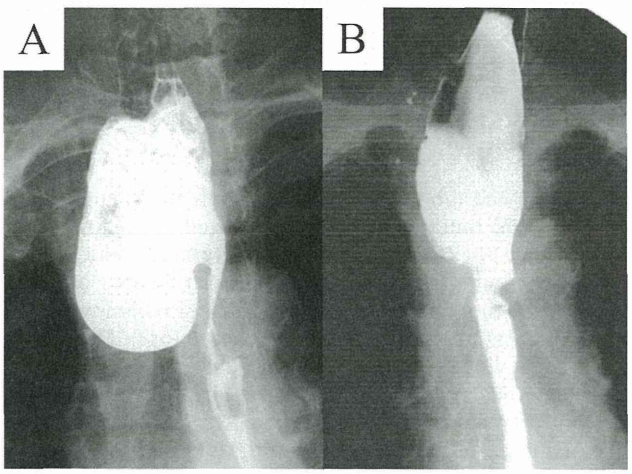

Fig 1. Preoperative and postoperative barium swallow radiographs. (A) Preoperative barium swallow radiograph shows significant retention of barium in a massive Zenker's diverticulum, reaching the carina (10.0 × 6.0 cm), with minimal conduction of barium into the distal esophageal lumen. (B) Postoperative barium swallow radiograph demonstrates free flow of barium into the esophagus and shrinkage of the hypopharyngeal dilatation.

Accepted for publication Aug 28, 2013.

Address correspondence to Dr Zhang, Department of Thoracic Surgery, Tianjin Chest Hospital, 93 Xi'an St, Tianjin 300051, China; e-mail: zhangxun69@163.com.

Published by Elsevier Inc

0003-4975/$36.00
http://dx.doi.org/10.1016/j.athoracsur.2013.08.063

Lung Cancer 83 (2014) 329–333

Contents lists available at ScienceDirect

Lung Cancer

journal homepage: www.elsevier.com/locate/lungcan

Analytical performance of the cobas EGFR mutation assay for Japanese non-small-cell lung cancer

Hideharu Kimura[a], Tatsuo Ohira[b], Osamu Uchida[c], Jun Matsubayashi[d], Shinichiro Shimizu[e], Toshitaka Nagao[d], Norihiko Ikeda[b], Kazuto Nishio[a,*]

[a] Department of Genome Biology, Kinki University Faculty of Medicine, 337-2 Ohno-Higashi, Osaka-Sayama, Osaka 589-8511 Japan
[b] Department of Surgery, Tokyo Medical University, 6-7-1 Nishi-shinjuku, Shinjuku-ku, Tokyo 160-0023, Japan
[c] Department of Respiratory Surgery, Funabashi Municipal Medical Center, 1-21-1 Kanasugi, Funabashi, Chiba 273-8588, Japan
[d] Department of Anatomic Pathology, Tokyo Medical University, 6-7-1 Nishi-shinjuku, Shinjuku-ku, Tokyo 160-0023, Japan
[e] Department of Pathology, Funabashi Municipal Medical Center, 1-21-1 Kanasugi, Funabashi, Chiba 273-8588, Japan

ARTICLE INFO

Article history:
Received 27 October 2013
Received in revised form
11 December 2013
Accepted 20 December 2013

Keywords:
Non-small-cell lung cancer
EGFR mutation
EGFR-TKI treatment
cobas® EGFR Mutation Test
Companion diagnostics
Personalised healthcare

ABSTRACT

Introduction: Clinical outcomes in non-small-cell lung cancer (NSCLC) patients with epidermal growth factor receptor (EGFR) mutations have been reported to be correlated with the use of EGFR-tyrosine kinase inhibitors (EGFR-TKIs). Therefore, it is essential to confirm the presence of EGFR mutations using highly sensitive testing methods. In this study, we compared the performance of the cobas® EGFR Mutation Test (cobas EGFR assay) and the *therascreen*® EGFR RGQ PCR Kit (*therascreen* EGFR assay) for use as an *in vitro* diagnostic (IVD) product.
Methods: We extracted DNA from 150 formalin-fixed, paraffin-embedded tissue samples from 150 patients diagnosed with NSCLC, and performed a comparative study of the cobas EGFR and *therascreen* EGFR assay methods. All discordant results were re-analyzed by direct sequencing.
Results: The concordance rate between the cobas EGFR assay and the *therascreen* EGFR assay was 98.0% (145/148). EGFR mutations were detected at a frequency of 40.9% (61/149) in NSCLC specimens using the cobas EGFR assay and 40.2% (60/149) using the *therascreen* EGFR assay. Three discrepant results were found in this study. Two double mutations were detected by the cobas EGFR assay but only one in the *therascreen* EGFR assay. No invalid results resulted from sample analysis by the cobas EGFR assay.
Conclusions: Our results show a high concordance rate (98.0%) of cobas EGFR assay with an existing IVD product, the *therascreen* EGFR assay. Since they are IVD diagnostic products, both assays proved to be simple, validated methods in detecting the most common, clinically significant EGFR mutations and proved to be helpful for appropriate treatment guidance for NSCLC patients.

1. Introduction

Non-small-cell lung cancer (NSCLC) patients frequently have activating EGFR mutations and respond well to treatment with small molecule EGFR-tyrosine kinase inhibitors (TKIs) such as gefitinib and erlotinib [1–4]. Both the American Society of Clinical Oncology and the Japan Lung Cancer Society recommend EGFR mutation testing in patients being considered for EGFR-TKI treatment as a first-line therapy [5]. Similar guidelines recommending testing for *EGFR* mutations were established by the College of American Pathologists, the International Association for the Study of Lung Cancer, and the Association for Molecular Pathology [6]. Patients' *EGFR* mutation status prior to the commencement of treatment impacts outcomes and, as a result, EGFR testing has been developed as a companion diagnostic; this relationship between therapeutic and diagnostic agents contributes to personalized healthcare. Recently, it was reported that about half of patients who are initially sensitive to EGFR-TKIs may acquire resistance to EGFR-TKIs [7] following a period of therapy, mainly as a result of the appearance of *EGFR* mutations associated with resistance to treatment, such as T790M. Indeed, a recent study suggested that the T790M mutation may be present in a small proportion of tumor cells prior to treatment, with the proportion of mutant alleles increasing gradually during treatment [8]. Similar findings were observed for exon 20 insertions; that they are usually associated with primary or de novo resistance to EGFR-TKI therapy [9]. Thus, it is important to re-assess *EGFR* mutation status during treatment to determine the most appropriate treatment regimens for patients.

A number of PCR-based techniques are used in the clinic for the assessment of *EGFR* mutations. In Japan, the "Scorpion-ARMS" *therascreen*® EGFR Rotor-Gene Q (RGQ) PCR Kit (*therascreen* EGFR

* Corresponding author. Tel.: +81 72 366 0221; fax: +81 072 367 6369.
E-mail address: knishio@med.kindai.ac.jp (K. Nishio).

0169-5002/$ – see front matter © 2014 Elsevier Ireland Ltd. All rights reserved.
http://dx.doi.org/10.1016/j.lungcan.2013.12.012

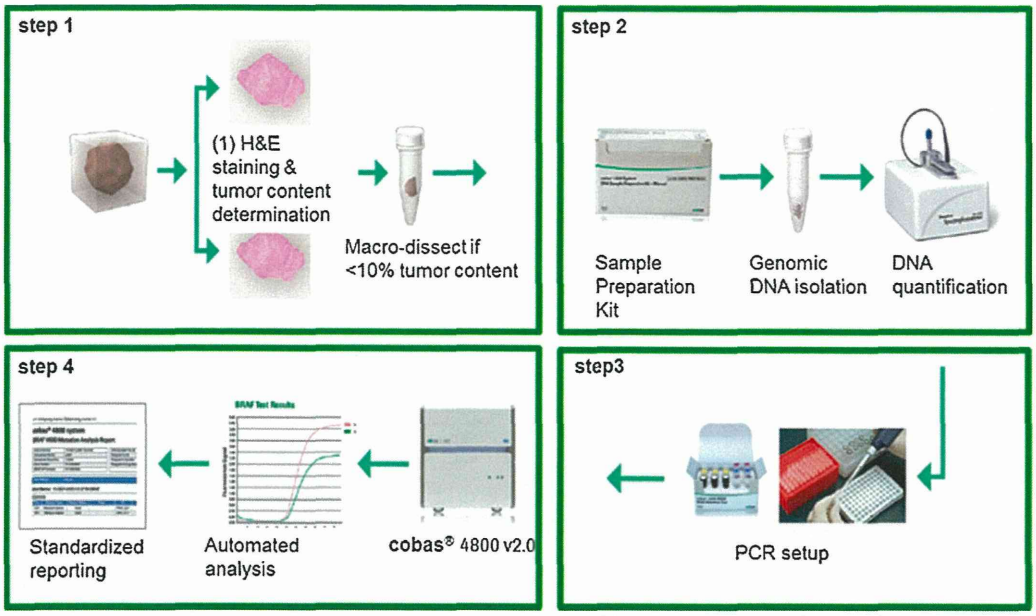

Fig. 1. Assay flow for the cobas EGFR mutation assay. The assay is composed of four steps. Step 1: 5-μm sections are prepared from FFPE tissue. One section is used for H&E staining to assess tumor content and the other section is used for DNA isolation. Step 2: Genomic DNA is isolated using the cobas® DNA Sample Preparation Kit. Step 3: DNA is mixed with reagents after quantification. Step 4: DNA is amplified using the cobas z 480 system. Results are automatically reported.

assay; Qiagen, Hilden, Germany) is the only available *in vitro* diagnostic (IVD) test.

In this study, we compared the performance of the cobas EGFR assay and the *therascreen* EGFR assay using formalin-fixed, paraffin-embedded (FFPE) tissue specimens from NSCLC patients.

2. Materials and methods

2.1. Tissue samples

A series of archived 150 FFPE tissue samples which was surgically resected from 150 Japanese patients diagnosed with NSCLC, collected between March 2011 and December 2012, was obtained from Tokyo Medical University (Tokyo, Japan) and Funabashi Medical Hospital (Funabashi, Japan). All patients enrolled in the study provided informed consent for the use of resected tissue. The study was approved by the ethics committee of each participating institute and conducted according to Institutional Review Board guidelines.

2.2. cobas EGFR Mutation Test

The cobas EGFR assay is an allele-specific real-time PCR system (Figure, Supplemental Digital Content 1; Fig. 1) that qualitatively measures the amplification of DNA to identify 41 mutations in exons 18–21 of the *EGFR* gene from 50 ng of DNA derived from human FFPE NSCLC tissues (Table, Supplemental Digital Content 2). Within each reaction mixture, exon 28 was amplified as an internal control. DNA isolation, amplification/detection, and result reporting can be performed in less than 8 h with up to 30 specimens processed simultaneously. The cobas EGFR assay has fully automated results reporting.

2.3. Specimen preparation for cobas EGFR assay

Two FFPE tissue sections of 5 μm thickness were prepared for this assay. One was used for DNA extraction and the other was used to confirm the presence of tumor content by hematoxylin and eosin (H&E) staining, which was performed by a pathologist. Any specimen containing <10% tumor content by area was macrodissected.

2.4. DNA extraction

FFPE tissue specimens were deparaffinized and then DNA extraction was performed according to the standard procedure described in the cobas® DNA Sample Preparation Kit (Roche Molecular Systems, Inc., USA) package insert. Briefly, the sample was incubated for 1 h at 56 °C and then for additional one hour at 90 °C in the presence of a protease and chaotropic lysis/binding buffer that causes the release of nucleic acids but protects released genomic DNA from degradation by DNase. The amount of genomic DNA was spectrophotometrically determined and adjusted to a fixed concentration of 2 ng/μL.

2.5. PCR amplification and detection

A total of 150 ng of DNA is required for the cobas EGFR assay. Target DNA was amplified and detected using the cobas® z480 analyzer (Roche Molecular Systems Inc.) according to the instructions for the cobas® EGFR Mutation Test, which measures the fluorescence generated by specific PCR products. All results were automatically performed by cobas® 4800 software.

2.6. therascreen® EGFR RGQ PCR Kit

The *therascreen* assay is a real time-PCR assay that combines the Amplification Refractory Mutation System (ARMS) and Scorpions fluorescent primer/probe system. It can detect 29 somatic mutations in exons 18–21 of *EGFR*. A maximum of 7 results can be obtained from one run. The *therascreen* EGFR assay was performed according to the manufacturer's guidelines (Qiagen). Briefly, DNA was isolated from FFPE tissue samples and the total sample DNA assessed by amplifying a region of exon 2 from *EGFR* by PCR. Next, the DNA samples were tested for the presence or absence of *EGFR* mutations by real-time PCR using a Scorpion probe and primers specific for wild type and mutant *EGFR* DNA. The difference

Table 1
Clinical characteristics of the patients providing surgically resected FFPE samples in NSCLC.

	N = 149
Gender	
Male	75
Female	74
Age	
Younger than 65 years	42
Older than 65 years	107
Histology	
Adenocarcinoma or adeno-squamous cell carcinoma (Ad)	126
Squamous cell carcinoma (Sq)	17
Large cell carcinoma (la)	2
Other	4
Smoking history	
Smoker	18
Ever smoker	73
Never smoker	56
ND	2

ND, not determined; N, number.

between the mutation assay cycle threshold (C_T) and control assay C_T from the same sample was used to calculate sample ΔC_T values. Samples designated mutation positive if the ΔC_T was less than the cutoff ΔC_T value.

2.7. Sanger sequencing

DNA samples obtained from specimens that were discordant between cobas EGFR and *therascreen* EGFR assays were amplified using the following site-specific primers: Exon 18 Forward, 5′-TGGAGCCTCTTACACCCAGT-3′, Reverse, 5′-ACAGCTTGCAAGGACTCTGG-3′; Exon 19 Forward, 5′-TCTGGATCCCAGAAGGTGAG-3′, Reverse, 5′-CAGCTGCCAGACATGAGAAA-3′; Exon 20 Forward, 5′-CATTCATGCGTCTTCACCTG-3′, Reverse, 5′-GTCTTTGTGTTCCCGGACAT-3′; Exon 21 Forward, 5′-GATCTGTCCCTCACAGCAGGGTC-3′, Reverse, 5′-GGCTGACCTAAAGCCACCTCC-3′. The fragments were subcloned into the Zero Blunt TOPO vector (Zero Blunt TOPO PCR Cloning Kit; Life Technologies, USA). Direct sequencing was performed with 100 colonies from one specimen by ABI3100 Genetic Analyzer (ABI) using the BigDye® Terminators v3.1 Cycle Sequencing Kit (Life Technologies). One mutation detected in 100 results was classed as "Mutation Detected" in this study. This assay required 1 μg of genomic DNA from specimens. Sanger sequencing was performed with the specimen that resulted double mutation (L858R and M790M) from cobas EGFR assay but single mutation (L858R) from *therascreen* EGFR assay at Mitsubishi Chemical Medicine Corporation followed by daily routine. The sequencing result was used as Golden standard.

3. Results

3.1. Study population

A series of 150 FFPE tissue samples from patients diagnosed with NSCLC was examined. One specimen was excluded owing to a lack of a completed consent form, leaving 149 samples available for analysis. The clinical and pathological characteristics of the patients providing the evaluable specimens are summarized in Table 1.

3.2. EGFR mutation types

EGFR mutations were identified in 63 NSCLC specimens (42.3%) using the cobas EGFR assay and 61 specimens (40.9%) using the *therascreen* EGFR assay (Table, Supplementary Digital Content 4). Exon 19 deletions (Ex19del) and a point mutation (L858R) accounted for 90.5% (57/63) and 93.4% (57/61) of all mutations identified using the cobas EGFR assay and *therascreen* EGFR assay, respectively (Table, Supplementary Digital Content 3). This confirms the findings of a previous study [10], which found that Ex19del and L858R mutations accounted for 90% of NSCLC *EGFR* activating mutations. The exon 20 insert mutation (Ex20Ins) was not observed in any of the samples tested in this study. A T790M point mutation was detected by the cobas EGFR assay (0.68%) but not by the *therascreen* EGFR assay.

Table 2
Methods correlation between mutation findings using the cobas EGFR and *therascreen* EGFR assays.

		therascreen			Total
		MD	MND	Invalid	
cobas	MD	59	2	0	61
	MND	1	86	1	88
	Invalid	0	0	0	0
	Total	60	88	1	149

MD, mutation detected; MND, mutation not detected.

Table 3
Detailed concordant rate between cobas EGFR and *therascreen* EGFR assays.

Mutation	MD concordance	MND concordance	Total concordance
G719X	100% (3/3)	100% (145/145)	100% (148/148)
exon19del	95.7% (22/23)	100% (125/125)	99.3% (146/147)
S768I	100% (1/1)	99.3% (146/147)	99.3% (147/148)
T790M	–	99.3% (147/148)	99.3% (147/148)
exon20ins	–	100% (148/148)	100% (148/148)
L858R	100% (34/34)	99.1% (113/114)	99.3% (147/148)

Del, deletion; Ins, insertion; MD, mutation detected; MND, mutation not detected.

3.3. Invalid test rate

Mutation analysis of exons 18–21 of the *EGFR* gene was successfully performed in all 149 specimens (100%) using the cobas EGFR assay. In contrast, in experiments using the *therascreen* EGFR assay, two test specimens initially gave invalid test results. In those cases, DNA was extracted from new FFPE tissue samples. However, because one sample gave an invalid result again, this case was excluded from the analysis, resulting in an invalid rate of 0.68% (1/148) for the *therascreen* EGFR assay (Table 2). In addition, one invalid control occurred in the *therascreen* EGFR assay (data not shown).

3.4. Method correlation agreement analysis

The correlation rate between cobas EGFR assay and *therascreen* EGFR assay was 98.0%. Of the 149 evaluable samples tested, only three discordants between the two EGFR mutation assays were observed (Table 3).

3.5. Re-analysis of discordants by direct sequencing

Test specimens that gave discordant results between the cobas EGFR and *therascreen* EGFR assays were retested using direct sequencing from sub-cloned samples (Table 4). A discordant MND by *therascreen* EGFR assay was observed by direct sequencing to be an L858R point mutation, confirming the MD result assessed by cobas EGFR assay. In addition, an Ex19del mutation identified as MD by *therascreen* EGFR assay was shown to be MND by direct sequencing, again confirming the cobas EGFR assay result. The cobas EGFR assay identified one case with a double mutation, L858R and T790M

Table 4
Re-analysis of discordants by direct sequencing.

	therascreen		Cobas		Sequencing (reanalysis)
Sample 1	MND	–	MD	L858R	MD
Sample 2	MD	EX19Del	MND	–	MND
Sample 3	MND	–	MD	S768I	MND
Sample 4	MD	L858R	MD	L858R,T790M	L858R

Del, deletion; Ins, insertion; MD, mutation detected; MND, mutation not detected.

Table 5
Re-analysis: combined *therascreen* EGFR assay and Sanger sequencing for resolution of discordant results.

		therascreen and/or Sanger sequencing	
		MD	MND
cobas	MD	60	1
	MND	0	87

MD, mutation detected; MND, mutation not detected.

(Table 4). However, only the L858R mutation was identified by the *therascreen* EGFR assay and only the T790M mutation was detected by direct sequencing. We then performed a re-analysis using a combination of the *therascreen* EGFR assay and Sanger sequencing for resolution of the discordant results (Table 5). This demonstrated an MD concordance rate of 100% (60/60), an MND concordance rate of 98.9% (87/88) and a total concordance rate of 99.3% (147/148) between the tests.

4. Discussion

The overall correlation results of the cobas EGFR assay, an existing EGFR mutation screening method (the *therascreen* EGFR assay) plus direct sequencing was 99.3% (147/148) (Table 5). It also indicated that the cobas assay is at least as robust method to detect the most common clinically significant EGFR mutations as the existing *therascreen* EGFR assay.

Although we identified 3 discordant results among 149 (2.0%) specimens in this study, retesting by direct sanger sequencing confirmed that two of the three discordant results were in fact correctly called by the cobas EGFR assay. Although both assays share similar characteristics in terms of amplification methods and detection principles, the slight differences (e.g. probe and primer construction) between the two of them, influenced their sensitivities to the mutations. Also, the remaining discordant result analysis highlighted the importance of the purity of the extracted DNA for the PCR amplification. In fact, an Ex 20 S768I mutation identified as Mutation Detected (MD) by the cobas EGFR assay but not the *therascreen* EGFR assay, was not detected by direct sequencing, either. In this case, direct sequencing failed more than two times to detect the EGFR gene when using the extracted DNA from the QIAmp DNA FFPE Tissue extraction kit (Qiagen) suggesting that the quality of the DNA was not adequate for the testing (data not shown). This potential difference in DNA quality might be the reason why we have experienced discordant results in some cases.

One T790M mutation was detected together with L858R by the cobas EGFR assay in this study. As there is known heterogeneity with regard to the T790M mutation within tumor cells, it is difficult to mention that the extracted DNA was completely the same, even if we used serial sections. However the raw data from the cobas system showed high enough signals to robustly detect the mutation (data not shown). According to the package insert, cobas EGFR needs at least 3.13 ng DNA which includes 5% mutated DNA to detect the mutation. Therefore it appears that the cobas test might be more sensitive than the *therascreen* test because, according to the *therascreen* package insert, it needs 7.02% mutated DNA within the input DNA [11,12].

About half of the patients who are initially sensitive to EGFR-TKIs may acquire resistance to EGFR-TKIs [7] following a period of therapy, mainly because of the selection for the cells with the T790M mutation in EGFR. In addition, the correlation between the presence of intrinsic T790M mutations and patient outcomes has been shown [8], and is probably related to the slow growth of tumors bearing the T790M mutation. Thus, it is important to re-assess EGFR mutation status during treatment in order to determine the most appropriate treatment regimens for patients.

For IVD products, it is important to have rapid and simple testing. The cobas EGFR assay has two advantages over the *therascreen* assay in this regard. One is that the process consists of easily performed and stable methods. Additionally, it takes only 8 h to go from tumor specimen to results using the semi-automated system. Thus, patients assessed using the cobas EGFR assay can begin the most appropriate treatment within a shorter time period. The other advantage is that only a very small amount of DNA (150 ng) is required to detect the tumor mutation status using the cobas EGFR assay. Moreover, it confirms the accuracy of the results by co-amplification of an internal control (i.e. exon 28). One of the issues associated with detecting EGFR mutations in advanced NSCLC patients is not obtaining a sufficient quantity of specimen to confirm the presence/absence of several biomarkers. It is important to be able to perform tests using just a small amount of DNA; thus, the cobas EGFR assay is suitable and reliable for the detection of targeted common EGFR mutations. In this study, we had high concordance with surgically resected specimens which had enough tumors. However, at clinical practice, minimal invisible samples such as pleural effusion or bronchial wash would be used from advanced NSCLC patients having difficulty of collecting tissue. To access this difficulty, even if the samples are small enough, at least confirming the amount of tumor cells by pathologist is required to have appropriate test result. Under the condition, it might be able to provide reliable result even if using either FFPE samples or cytology samples. It is important to accumulate the data with cytology samples which makes improvement of suitable testing for advanced NSCLC patients in the future.

5. Conclusion

In the near future, more mutations that can serve as predictive markers for molecular-targeted treatments will be discovered, and mutation detection tests will play an increasingly important role in the clinical setting. The benefits of treatment will be maximized only if used together with clinically validated and accurate companion diagnostics. The cobas system offers the possibility of detecting additional mutations, not only mutations of EGFR. The combination of the cobas system with molecular-targeted treatments represents an important tool for physicians, supporting their efforts to effectively treat tumors.

Conflict of interest

Hideharu Kimura, Tatsuo Ohira, Osamu Uchida, Jun Matsubayashi, Shinichirou Shimizu, Toshitaka Nagao, Kazuto Nishio, Norihiko Ikeda was funded by Roche Diagnostics K.K. (Tokyo, Japan). There was no other financial support for the investigators.

Acknowledgements

This study was sponsored by Roche Diagnostics K.K. This means that the publication of this study is written by investigators and has no relative value of the cobas EGFR test for the promotion.

Appendix A. Supplementary data

Supplementary data associated with this article can be found, in the online version, at http://dx.doi.org/10.1016/j.lungcan.2013.12.012.

References

[1] Zhou C, Wu YL, Chen G, Feng J, Liu XQ, Wang C, et al. Erlotinib versus chemotherapy as first-line treatment for patients with advanced EGFR mutation-positive non-small-cell lung cancer (OPTIMAL, CTONG-0802): a multicentre, open-label, randomised, phase 3 study. Lancet Oncol 2011;12:735–42.

[2] Mok TS, Wu YL, Thongprasert S, Yang CH, Chu DT, Saijo N, et al. Gefitinib or carboplatin-paclitaxel in pulmonary adenocarcinoma. N Engl J Med 2009;361:947–57.

[3] Rosell R, Carcereny E, Gervais R, Vergnenegre A, Massuti B, Felip E, et al. Erlotinib versus standard chemotherapy as first-line treatment for European patients with advanced EGFR mutation-positive non-small-cell lung cancer (EURTAC): a multicentre, open-label, randomized phase 3 trial. Lancet Oncol 2012;13:239–46.

[4] Maemondo M, Inoue A, Kobayashi K, Sugawara S, Oizumi S, Isobe H, et al. Gefitinib or chemotherapy for non-small-cell lung cancer with mutated EGFR. N Engl J Med 2010;362:2380–8.

[5] Keedy VL, Temin S, Somerfield MR, Beasley MB, Johnson DH, McShane LM, et al. American Society of Clinical Oncology provisional clinical opinion: epidermal growth factor receptor (EGFR) mutation testing for patients with advanced non-small-cell lung cancer considering first-line EGFR tyrosine kinase inhibitor therapy. J Clin Oncol 2011;29: 2121–7.

[6] Lindeman NI, Cagle PT, Beasley MB, Chitale DA, Dacic S, Giaccone G, et al. Molecular testing guideline for selection of lung cancer patients for EGFR and ALK tyrosine kinase inhibitors: guideline from the College of American Pathologists, International Association for the Study of Lung Cancer, and Association for Molecular Pathology. J Thorac Oncol 2013;(April) [Epub ahead of print].

[7] Nguyen KS, Kobayashi S, Costa DB. Acquired resistance to epidermal growth factor receptor tyrosine kinase inhibitors in non-small-cell lung cancers dependent on the epidermal growth factor receptor pathway. Clin Lung Cancer 2009;10:281–9.

[8] Fujita Y, Suda K, Kimura H, Matsumoto K, Arao T, Nagai T, et al. Highly sensitive detection of EGFR T790M mutation using colony hybridization predicts favorable prognosis of patients with lung cancer harboring activating EGFR mutation. J Thorac Oncol 2012;7:1640–4.

[9] Yasuda H, Kobayashi S, Costa DB. EGFR exon 20 insertion mutations in non-small-cell lung cancer: preclinical data and clinical implications. Lancet Oncol 2012;13:e23–31.

[10] Sharma SV, Bell DW, Settleman J, Haber D. Epidermal growth factor receptor mutations in lung cancer. Nat Rev Cancer 2007;7:169–81.

[11] Roche Molecular System Inc. cobas EGFR Mutation Test CE-IVD [Package Insert]. Branchburg, NJ, USA: Roche Molecular Systems Inc.; 2011.

[12] QIAGEN Manchester Ltd. *therascreen* EGFR RGQ PCR Kit Handbook; 2012.

Gen Thorac Cardiovasc Surg (2014) 62:720–725
DOI 10.1007/s11748-014-0441-7

ORIGINAL ARTICLE

Initial results of robot-assisted thoracoscopic surgery in Japan

Hiroshige Nakamura · Takashi Suda · Norihiko Ikeda · Morihito Okada · Hiroshi Date · Makoto Oda · Akinori Iwasaki

Received: 6 May 2014 / Accepted: 13 June 2014 / Published online: 18 July 2014

Abstract
Objectives As surgical robots have become increasingly used, verification of their usefulness in the general thoracic surgery field is required. Initial results of robot-assisted thoracoscopic surgery in Japan were investigated.
Methods A questionnaire survey was performed to retrospectively examine the current status of robotic surgery for general thoracic disease in Japan. The subjects were 112 cases performed by the end of September 2012 at 9 institutions.
Results There were 60 cases of primary lung cancer, 38 cases of anterior-middle mediastinal disease, and 14 cases of posterior mediastinal disease. In lung cancer cases, the operative time was 284.7 min, the blood loss was 129 mL, the drainage period was 3.3 days, and the conversion rate was 3.3 %. The incidence of postoperative complications was 6.7 %. The postoperative hospital stay was 8.2 days. In cases of anterior-middle mediastinal disease, the operative time was 184.3 min, the blood loss was 43.8 mL, the drainage period was 2.3 days, and there was no conversion. The incidence of postoperative complications was 7.9 %. The postoperative hospital stay was 7.1 days. In cases of posterior mediastinal disease, the operative time was 142.6 min, the blood loss was 61.4 mL, the drainage period was 1.6 days, and there was no conversion. No postoperative complication developed in any case. The postoperative hospital stay was 5 days. In all cases underwent robotic surgery, there was no operation related mortality.
Conclusions Robotic surgery was safely introduced, and the incidence of postoperative complications tended to be low, although the operative time was long. Preparations for its employment in advanced medical care and coverage by national health insurance are urgent issue.

Keywords Robot-assisted thoracoscopic surgery · da Vinci · Initial results

H. Nakamura · T. Suda · N. Ikeda · M. Okada · H. Date · M. Oda · A. Iwasaki
Research Committee of Robotic Surgery for General Thoracic Disease, Japanese Association for Chest Surgery, Kyoto, Japan

H. Nakamura (✉)
Division of General Thoracic Surgery, Department of Surgery, Faculty of Medicine, Tottori University, 36-1 Nishi-cho, Yonago, Tottori 683-8504, Japan
e-mail: hnaka@med.tottori-u.ac.jp

Introduction

A surgical robot, da Vinci, was introduced into the market by Intuitive Surgical, Inc. of USA in 1999. Modifications were made thereafter, and the Pharmaceutical Affairs Council of the Ministry of Health, Labour and Welfare approved da Vinci S in November 2009, and the latest model, da Vinci Si, in October 2012 in Japan. Their characteristics are: (1) 3-dimensional visual field that can be magnified up to 10 times, (2) articulated joint forceps with 7 degrees of freedom, and (3) prevention of camera shake using a motion scaling function. These facilitate the accurate and simple application of complex surgical techniques in a narrow field, realizing sophisticated surgery [1, 2]. As the dissemination of surgical robots progresses, verification of their usefulness in the general thoracic surgery field is required. We report the initial results in Japan and discuss problems.

Patients and methods

The Committee for robot-assisted surgery of the Japan Society for Endoscopic Surgery performed a questionnaire

survey on the current state of a robot-assisted surgery performed by the end of September 2012 in Japan in institutions possessing a robot-assisted surgical system, da Vinci (Intuitive Surgical Company, CA, USA). Questionnaire was consisted of 34 items, including patient and disease profile, operative procedure, operation time, preparation time, console time, bleeding amount, conversion case, postoperative complications, prognosis, and so on (Fig. 1). In the general thoracic surgery field, 9 institutions (Tottori University Hospital, Fujita Health University Hospital, Tokyo Medical University Hospital, Hiroshima University Hospital, Kyoto University Hospital, Tokyo Women's Medical University Hospital, Kyusyu University Hospital, Kanazawa University Hospital and Tokushima University Hospital) replied, and a total of 112 cases (33, 22, 20, 11, 10, 5, 4, 4, and 3 cases, respectively) were collected and included in this study. There were 60 cases of primary lung cancer, 38 cases of anterior-middle mediastinal disease, and 14 cases of posterior mediastinal disease. Regarding the details of operative method, those depended on the institutional policy except for using surgical robot for intrathoracic procedures. Perioperative data of these cases were mainly analyzed retrospectively. The study design was approved by the appropriate ethics review boards in each institution.

Results

The clinicopathological background of the patients who underwent robotic surgery and their perioperative outcomes are summarized in Tables 1 and 2, respectively. The outcomes of patients with primary lung cancer, anterior-middle mediastinal disease, and posterior mediastinal disease are separately described below.

Robot-assisted surgery for primary lung cancer

The mean age of the 60 primary lung cancer patients was 64.5 years, and there were 32 males and 28 females. The most common histologic type was adenocarcinoma (53 cases, 88 %). The clinical stage was I in 54, accounting for 90 %, but the number of pathological stage I cases decreased to 48 (80 %). The surgical procedure was lobectomy in 56 (93 %), accounting for the majority: resection of the right upper lobe in 22, the right middle lobe in 7, right lower lobe in 14, left upper lobe in 8, and left lower lobe in 6, including one case of bronchoplasty of the right upper lobe, and 3 cases of segmentectomy (right S6, left upper segment, and left basal segment in one each). The operative time was 284.7 min, the console time was 206.4 min, and the blood loss was 129 mL. The operative time was long because they were initial cases. The procedure was converted to thoracotomy in 2 (3.3 %) because of hemorrhage. The blood loss reached 2,069 mL in one case, and blood transfusion was performed. The drainage period was 3.3 days, and postoperative complications occurred in 4 (6.7 %): pulmonary fistula, chylothorax, atrial fibrillation, and cholecystitis in one patient each. All were mild and graded 2 with the Clavien–Dindo classification. No 30-day postoperative mortality occurred. The durations of postoperative and total hospital stays were 8.2 and 10.9 days, respectively. During the average follow-up period of 16.8 months, the disease recurred in 4 (6.7 %)

Fig. 1 Questionnaire items

1. Age
2. Gender
3. Body size
4. Performance status
5. Disease
6. Stage
7. Cormorbidity
8. ASA-PS
9. Operative date
10. Operative procedure
11. Operative time
12. Console time
13. Set up time
14. LN dissection time
15. Number of dissected hilar LN
16. Number of dissected mediastinal LN
17. Number of used robotic arms
18. Use of CO_2 insufflation
19. Instrument
20. Devise
21. Bleeding amount
22. Transfusion
23. Conversion case
24. da Vinci disorder
25. Console and Assistant surgeon
26. Postoperative complication
27. Duration of drainage period
28. Postoperative hospital stay
29. Hospital stay
30. Weight of resected specimen
31. Pathological diagnosis
32. Pathological stage
33. Evaluation of postoperative pain
34. Prognosis